FLAPW goes Non-collinear

Ph. Kurz, G. Bihlmayer, F. Förster, S. Blügel[+]
Institut für Festkörperphysik, Forschungszentrum Jülich,
D-52425 Jülich, Germany

L. Nordström
Condensed Matter Theory Group, Physics Department, Box 530,
Uppsala University, Uppsala, Sweden

Introduction

Non-collinear magnetism in general and incommensurate spin-density waves in particular are complex magnetic structures which exist in a variety of systems. They often occur for topologically frustrated antiferromagnets (e.g. antiferromagnets on a triangular lattice) or materials with competing exchange interactions as for example in the lanthanides. Non-collinear magnetism occurs in spin-glass systems, in domain walls, and is natural for spin fluctuations at finite temperature. The magnetic properties of complex magnets are commonly described within the framework of model Hamiltonians, the simplest of which is the classical Heisenberg model.

In the last years we witnessed a multitude of investigations of non-collinear magnetism in the context of first-principles theory. For instance several *ab initio* calculations have been presented for fcc Fe [1, 2, 3, 4], where solutions of both the spiral spin-density wave and complex non-collinear magnetic structures have been found. Non-collinear magnetic ground states have also been found for more complicated systems such as $MnSn_3$ [5], $ThMn_2$ [6], U_3P_4, U_2Pd_2Sn [7], $YFe_{12-x}Mo_x$ [8], disordered systems [8, 9, 10, 11], multilayers [12, 13] and molecular magnets [14]. Recently, interesting steps have been undertaken to describe the spin-dynamics in itinerant magnets [4, 15]. After the thorough discussion of density functional theory for a non-collinear magnet was completed in [5], these calculations established the density functional theory as a powerful tool to investigate these systems. For a general review see Psi-k Newsletter 14 [16] or the paper by Sandratskii [17].

Common to all of these calculations, which have been carried out using a variety of methods, such as the Korringa-Kohn-Rostoker (KKR) method [1, 18], the Augmented Spherical Wave

(ASW) method [19, 20, 5] or the Linear Muffin Tin Orbital (LMTO) [2, 21] method, is the use of the atomic sphere approximation. That means the space is divided into spheres centered around each atom, wherein there is only one local spin-quantization axis and the corresponding magnetization axis is spherically averaged, $\mathbf{m}(\mathbf{r}) \approx m(r)\hat{\mathbf{e}}_M$. This is consistent with the intuitive picture that each atom carries a magnetic moment and these moments (and their directions) differ between the atoms. Such methods are very suitable to describe the inter-atomic non-collinearity of close-packed systems.

There are, however, problems which call to go beyond the atomic sphere-type of approximation. One of those problems is the investigation of the intra-atomic non-collinear magnetism. This has been pioneered by Nordström *et al.* [22, 23]. Using the full-potential linearized augmented plane wave method (FLAPW), which is free of any shape approximation of the charge- and magnetization density as well as of the potential, the intra-atomic non-collinearity was described taking the full continuous vector spin-density $\mathbf{m}(\mathbf{r})$ into account as it was originally formulated by von Barth and Hedin [24]. It was shown for δ-Pu that due to the interplay of spin-orbit interaction and exchange interaction intra-atomic non-collinearity exists even for ferromagnets.

The frontier field of nanomagnetism creates a second class of interesting problems. In this case we deal with non-collinear magnetism in fairly open structures for which the atomic sphere approximation is known to be less suitable and often provides results with insufficient accuracy. Typical problems are exchange-bias systems [25], technologically important for the magnetic recording industry and the magneto-electronics [26], made out of ferromagnetic films adjacent to antiferromagnetic ones. Recently, we have made an effort to explore this subject using the FLAPW-method, but any other full-potential method capable to deal with magnetism would be equally suitable. In order to deal with non-collinear magnetism of these systems, the Jülich group has extended the film and bulk FLAPW-program `FLEUR` [27] along several directions [28]: (i) to deal with magnetic moments oriented along arbitrary and prescribed directions $\hat{\mathbf{e}}_M^\alpha$ for each atom α, (ii) to deal with the incommensurate spin-spiral state, (iii) and to relax the direction of the magnetic moment self-consistently.

In the following we shortly discuss the implementation of the vector spin-density formalism into the FLAPW-program and go briefly through items (i) and (iii). (ii) the implementation of the spin-spiral states has been nicely discussed in the paper of Andersson *et al.* [29] and is not further mentioned here. At the end we discuss one application, the magnetic spin-structure or an antiferromagnetic monolayer on a triangular lattice: Cr/Ag(111) and Mn/Ag(111).

Implementation of continuous vector spin-density formulation

Non-collinear magnetism has been implemented into two FLAPW codes choosing alternative strategies: Nordström *et al.* [22] work with more physical quantities, the density $n(\mathbf{r})$ and the magnetization density $\mathbf{m}(\mathbf{r})$, and with a spin-independent LAPW basis-set but extended by spin-dependent local orbitals. The implementation of the Jülich group is based on the spin-density matrices and on the standard LAPW basis-set using spin-dependent radial wave functions $u_{\ell\sigma}(r)$ and their energy derivative $\partial u_{\ell\sigma}(r)/\partial E$. The biggest difference, however, arises from the motivation that Jülich group is predominantly interested in the non-collinear magnetism

of $3d$ transition metals at surfaces and in open structures. These are elements with weak intra-atomic non-collinearity. Typically $\mathbf{m}(\mathbf{r})$ is well localized inside the atomic sphere, where $\mathbf{m}(\mathbf{r})$ is essentially parallel to the average of the spin-density of the sphere except in regions close to the sphere boundary where $\mathbf{m}(\mathbf{r})$ is already small. Since in the FLAPW-method the muffin-tin spheres are used which are significantly smaller than volume filling atomic spheres and since the choice of the sphere radii is flexible to a certain degree, but definitely smaller than half the nearest-neighbor distance, we work with a hybrid method: The magnetization is treated as a continuous vector field in the interstitial region and in the vacuum, while inside each muffin-tin sphere we only allow for one direction of magnetization

$$\mathbf{m}(\mathbf{r}) = \begin{cases} \mathbf{m}(\mathbf{r}) & \text{Interstitial and Vacuum} \\ \\ m^{\alpha}(\mathbf{r})\,\hat{\mathbf{e}}_M^{\alpha} & \text{muffin-tin sphere } \alpha \end{cases} . \tag{1}$$

The notation here applies to the FLAPW in the film geometry [30], where the space is partitioned into a film of finite thickness, consisting of an interstitial region and muffin-tin spheres α, and two semi-indefinite vacuum regions on both sides of the film. The continuous vector-field description in the interstitial region describes to a large extent the intra-atomic magnetism of $3d$-metals. This "hybrid" approach is illustrated schematically in Fig. 1.

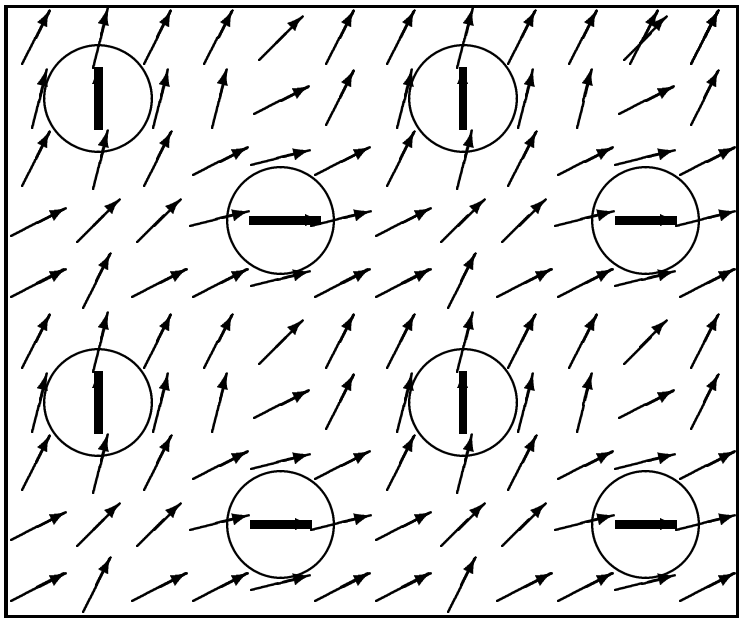

Figure 1: Schematic illustration of the representation of the non-collinear magnetization density within the present approach. The magnetization is treated as a continuous vector field in the interstitial region and in the vacuum. Within each muffin-tin the magnetization has a fixed direction (thick arrows) and can only vary in magnitude. For a better illustration the muffin-tin spheres have been chosen much smaller than in actual calculations.

For chemical elements with a large spin-orbit interaction or off-diagonal intra-atomic Coulomb interaction, one should extend the method to the full vector-field treatment of the magnetization density everywhere in space. To achieve this, it would be necessary to calculate the components of the magnetization that are not parallel to the local quantization axis in the sphere of an atom

and to include the corresponding components of the B-field into the Hamiltonian.

The FLAPW method for collinear calculation uses two sets of radial basis functions inside the muffin-tins for the spin directions. For each spin direction they are set-up using the spherical part of the corresponding potential, $V_\uparrow(r)$ or $V_\downarrow(r)$, and energy parameter, $E_{l\uparrow}$ or $E_{l\downarrow}$. It is still possible to work with $V_\uparrow(r)$ and $V_\downarrow(r)$ in the non-collinear case, since we restrict the magnetization to the local quantization axis. Therefore, a local spin space coordinate frame is introduced with the z-axis parallel to the local quantization axis. $V_\uparrow$ and $V_\downarrow$ are now spin-up and -down with respect to the local axis. Since both, the potential and the basis functions, are set up in terms of the local spin coordinate frame the determination of the basis functions and calculation of the integrals of these functions with the Hamiltonian inside the muffin-tin spheres is completely unchanged. The changes come in, when the basis functions inside the muffin-tins are matched to the plane waves in the interstitial region, because the local spin coordinate frame S^α is rotated with respect to the global frame S^g.

The FLAPW method uses augmented plane waves as basis functions. Therefore, each basis function can be uniquely identified by its wave vector $\mathbf{G}$ and the spin direction. The basis functions in the interstitial region are:

$$e^{i(\mathbf{k}+\mathbf{G})\mathbf{r}}\chi_\sigma^g, \tag{2}$$

χ_σ^g is a two component spinor. The index g has been added to notify that χ_σ^g is the representation of this spinor in the global spin frame. This representation is used for both collinear and non-collinear calculations. However in the collinear case, the potential matrix $\mathbf{V}$, and thus the Hamiltonian is block-diagonal in the space spanned by the two spin directions. Therefore, the Hamiltonian can be set-up and solved separately for each of the two spin directions (blocks). In the non-collinear case, $\mathbf{V}$ has off-diagonal parts which are not zero anymore. Hence, the full Hamiltonian for both spin directions are set-up and solved in a single step. In the vacuum region we also use the global spin frame for the representation of the basis functions. Only inside the muffin-tin spheres the basis set is changed, because we use a local spin-coordinate frame, which is rotated with respect to the global frame. The consequence is that, when the functions in the sphere are matched to the plane waves at the boundary of the muffin-tin spheres, each spin direction in the interstitial region is matched to both, the spin-up and -down basis functions, in the sphere. Thus, the basis set has the following form:

$$\varphi_{\mathbf{G},\sigma}(\mathbf{k},\mathbf{r}) = \begin{cases} e^{i(\mathbf{G}+\mathbf{k})\mathbf{r}}\ \chi_\sigma^g & \text{Int.} \\ \left[A_\sigma^{\mathbf{G}}(\mathbf{k}_\parallel)\, u_\sigma^{\mathbf{G}_\parallel}(\mathbf{k}_\parallel,z) + B_\sigma^{\mathbf{G}}(\mathbf{k}_\parallel)\, \dot{u}_\sigma^{\mathbf{G}_\parallel}(\mathbf{k}_\parallel,z)\right] e^{i(\mathbf{G}_\parallel+\mathbf{k}_\parallel)\mathbf{r}_\parallel}\ \chi_\sigma^g & \text{Vac.} \\ \displaystyle\sum_{\sigma^{\mu(\alpha)}}\sum_L \left[A^{\alpha\mathbf{G}}_{L\sigma\sigma^{\mu(\alpha)}}(\mathbf{k})\, u^{\alpha(\mu)}_{\ell\sigma^{\mu(\alpha)}}(r) + B^{\alpha\mathbf{G}}_{L\sigma\sigma^{\mu(\alpha)}}(\mathbf{k})\, \dot{u}^{\mu(\alpha)}_{\ell\sigma^{\mu(\alpha)}}(r)\right] Y_L(\hat{\mathbf{r}})\ \chi_{\sigma^{\mu(\alpha)}} & \text{MT}\alpha \end{cases} \tag{3}$$

where $\mathbf{k}$ is the Bloch vector, $\mathbf{G}$ is a reciprocal lattice vector, L abbreviates the quantum numbers l and m, u_l is the regular solution of the radial Schrödinger equation, and $\dot{u}_l$ denotes the energy derivative of u_l. The A- and B-coefficients are determined from the requirement, that the wavefunctions and their derivative have to be continuous at the sphere boundary. The sum in the muffin-tin spheres is over the local spin directions.

After the generalized eigenvalue problem including the full Hamiltonian and overlap matrix

for both spin directions is solved, we obtain the eigenstates of the non-collinear system. The eigenstates are given in terms of the basis functions (3).

$$\psi_\nu(\mathbf{k},\mathbf{r}) = \sum_\sigma \sum_{\mathbf{G}} \mathbf{c}^{\mathbf{G}}_{\nu,\sigma}(\mathbf{k}) \varphi_{\mathbf{G},\sigma}(\mathbf{k},\mathbf{r}). \tag{4}$$

Now the density matrix in the (2×2) spin-space

$$\rho = \frac{1}{2}(n\ I_2 + \boldsymbol{\sigma}\cdot\mathbf{m}) \tag{5}$$

is given by a very simple relation in terms of the solutions of the eigenfunctions

$$\rho_{\alpha\beta} = \sum_{\nu=1}^{N} \psi^*_{\nu,\alpha}\psi_{\nu,\beta}. \tag{6}$$

The potential matrix is defined the same way

$$\mathbf{V} = V\ I_2 + \boldsymbol{\sigma}\cdot\mathbf{B}. \tag{7}$$

Due to the non-collinear magnetism the Hamiltonian has twice the dimension as for the collinear case, the matrix is hermitian, the unit cells become large, the symmetry can become fairly low and often different magnetic states have very similar energies, which requires a large amount of k-points to energetically resolve such magnetic states. Thus the calculations can become rather demanding and the computer codes are parallelized with respect to the number of k-points and eigenstates ν.

Constraint local moments

In general [except for some high symmetry magnetic states e.g. the ferromagnetic state or a particular class of spin-spiral states], an arbitrary magnetic configuration prescribed by a set of magnetization directions $\{\hat{\mathbf{e}}^\alpha_M\}$ are not extrema to the total energy functional $E[n(\mathbf{r}),\mathbf{m}(\mathbf{r})]$. To ensure that the local moments have no components $M^\alpha_\perp$ normal to the directions $\hat{\mathbf{e}}^\alpha_M$, $\hat{\mathbf{e}}^\alpha_\perp$, we work with the constrained DFT [31] in which the total energy for a set of prescribed directions $E(\{\hat{\mathbf{e}}^\alpha_M\})$ is solved, subject to the orientational constraint of the magnetic moments, that $\langle\mathbf{m}^\alpha\rangle\times\hat{\mathbf{e}}^\alpha_M$ is zero for all atoms,

$$E(\{\hat{\mathbf{e}}^\alpha_M\}) = \min\Big\{E[n(\mathbf{r}),\mathbf{m}(\mathbf{r})] + \sum_\alpha \mathbf{B}^\alpha_\perp \langle\mathbf{m}^\alpha\rangle\times\hat{\mathbf{e}}^\alpha_M\Big\}. \tag{8}$$

The Lagrange multipliers $\mathbf{B}^\alpha_\perp$ are transverse constraining fields in the direction $\hat{\mathbf{e}}^\alpha_\perp$. They are obtained self-consistently, simultaneously with the densities. At the end of such a calculation we obtain the self-consistent densities and a set of local constraining B-fields $\{\mathbf{B}^\alpha_\perp\}$ that make the integrated magnetization $\langle\mathbf{m}^\perp_i\rangle$, perpendicular to the local spin quantization axes $\hat{\mathbf{e}}^\alpha_M$, vanish in each muffin-tin sphere.

The effective B-field, $\mathbf{B}^\alpha_{eff}$, that enters the muffin-tin part of the Hamiltonian is given by

$$\mathbf{B}^\alpha_{eff}(\mathbf{r}) = B^\alpha_{xc}\Big(n(\mathbf{r}),m_{\|}(\mathbf{r})\Big)\,\hat{\mathbf{e}}^\alpha_M\ +\ B^\alpha_\perp\,\hat{\mathbf{e}}^\alpha_\perp = B^\alpha_{xc}(\mathbf{r})\,\hat{\mathbf{e}}^\alpha_M\ +\ B^\alpha_\perp\,\hat{\mathbf{e}}^\alpha_\perp = \mathbf{B}^\alpha_{eff}(\mathbf{r})\,\hat{\mathbf{e}}^\alpha_B(\mathbf{r}). \tag{9}$$

In order to calculate the exchange correlation B-field, $\mathbf{B}^\alpha_{xc}(\mathbf{r})$, after the magnetization density is calculated from the wave functions, the magnetization density is projected onto the prescribed local quantization axis $\hat{\mathbf{e}}^\alpha_M$ and we obtain $m^\alpha_\parallel(\mathbf{r})$. Since the exchange correlation B-field is calculated from the projected magnetization density, it is collinear. However, when a constraining field is added, the resulting effective B-field, $\mathbf{B}^\alpha_{eff}(\mathbf{r})$, is again a continuous non-collinear vector field in the muffin-tin spheres, with pointwise local directions $\hat{\mathbf{e}}^\alpha_B(\mathbf{r})$,

$$\hat{\mathbf{e}}^\alpha_B(\mathbf{r}) = \frac{B^\alpha_{xc}(\mathbf{r})\,\hat{\mathbf{e}}^\alpha_M + B^\alpha_\perp\,\hat{\mathbf{e}}^\alpha_\perp}{\left((B^\alpha_{xc}(\mathbf{r}))^2 + (B^\alpha_\perp)^2\right)^{\frac{1}{2}}}, \tag{10}$$

different from the local quantization axis $\hat{\mathbf{e}}^\alpha_M$. Stocks *et al.* [15] noticed this problem and approximated $B^\alpha_\perp$ by an $\mathbf{r}$-dependent functional form $B^\alpha_\perp = c^\alpha\, B^\alpha_{xc}(\mathbf{r})$, where c^α replaces $B^\alpha_\perp$ as the parameter to be determined. This approximation simplifies $\hat{\mathbf{e}}^\alpha_B(\mathbf{r})$ to $\hat{\mathbf{e}}^\alpha_B(\mathbf{r}) \approx \hat{\mathbf{e}}^\alpha_B = (\hat{\mathbf{e}}^\alpha_M + c^\alpha\hat{\mathbf{e}}^\alpha_\perp)/\sqrt{1+(c^\alpha)^2}$, and $\mathbf{B}^\alpha_{eff}(\mathbf{r}) = \sqrt{1+(c^\alpha)^2}\,B_{xc}(\mathbf{r})\,\hat{\mathbf{e}}^\alpha_B$ becomes again collinear within each sphere. The constraining B-fields, $\mathbf{B}^\alpha_\perp$, that enter are often rather small and the approximation suggested by Stocks might be a very good one, although we have not further investigated that. On the other hand due to the introduction of the $\mathbf{r}$-dependence in the constraining fields, the approximation makes the constraining fields inconsistent with the defining equation, Eq. 8. Therefore, we introduce a collinear effective B-field, $\mathbf{B}^\alpha_{eff}(\mathbf{r}) = B^\alpha_{eff}(\mathbf{r})\langle\hat{\mathbf{e}}^\alpha_B\rangle$ in the sphere, by approximating $\hat{\mathbf{e}}^\alpha_B(\mathbf{r})$ by its average direction over the muffin-tin sphere $\langle\hat{\mathbf{e}}^\alpha_B\rangle$, which is independent of $\mathbf{r}$. $\langle\hat{\mathbf{e}}^\alpha_B\rangle = (\hat{\mathbf{e}}^\alpha_M + c^\alpha\hat{\mathbf{e}}^\alpha_\perp)/\sqrt{1+(c^\alpha)^2}$ is defined by replacing the exchange correlation B-field $B_{xc}(r)$ in Eq. 10 by its average over the muffin-tin sphere, $\langle B_{xc}\rangle$, and c^α is now defined as the ratio $c^\alpha = B^\alpha_\perp/\langle B_{xc}\rangle$. For this choice of direction for the effective B-field, the average effective B-field perpendicular to $\langle\hat{\mathbf{e}}^\alpha_B\rangle$, $\langle\hat{\mathbf{e}}^\alpha_B\rangle_\perp$, is zero, $\langle\mathbf{B}^\alpha_{\perp,eff}\rangle = 0$.

Summarizing we can write

$$\mathbf{B}^\alpha_{eff}(\mathbf{r}) = \frac{1}{\sqrt{1+(c^\alpha)^2}}(B^\alpha_{xc}(\mathbf{r}) + c^\alpha B^\alpha_\perp)\langle\hat{\mathbf{e}}^\alpha_B\rangle \qquad \text{with} \qquad \langle\hat{\mathbf{e}}^\alpha_B\rangle = \frac{1}{\sqrt{1+(c^\alpha)^2}}(\hat{\mathbf{e}}^\alpha_M + c^\alpha\hat{\mathbf{e}}^\alpha_\perp). \tag{11}$$

Thus in constrained local moment calculations one works with two slightly different local spin coordinate frames. One of them is given by the direction $\hat{\mathbf{e}}^\alpha_M$ to which the local moment is constrained to, and the other is defined by the average direction $\langle\hat{\mathbf{e}}^\alpha_B\rangle$ of the effective B-field. After the eigenvalue problem has been solved, the solutions are represented within the spin coordinate frame defined by $\langle\hat{\mathbf{e}}^\alpha_B\rangle$, since the Hamiltonian has been setup within that coordinate frame. Hence, when the density matrix is constructed, it is also given with respect to that frame. In order to obtain the density matrix in the spin frame defined by $\hat{\mathbf{e}}^\alpha_M$, it needs to be rotated. To achieve this we first apply the spin-rotation matrix that rotates the density matrix from the coordinate frame $\langle\hat{\mathbf{e}}^\alpha_B\rangle$ to the global spin frame, and then we rotate it again from the global frame to the frame given by $\hat{\mathbf{e}}^\alpha_M$.

Relaxation of the orientation of magnetic moments

In the previous section we have explained how a calculation can be performed where the local magnetic moments are constrained to a set of prescribed directions $\hat{\mathbf{e}}^\alpha_M$. In this section we will show, how the magnetic configuration given by the $\hat{\mathbf{e}}^\alpha_M$ can be relaxed to find a (local) minimum

of the total energy $E\{\hat{\mathbf{e}}_M^\alpha\}$. In such a calculation we also apply the approximation of a collinear magnetization density inside each muffin-tin sphere, $\mathbf{m}(\mathbf{r}) = m^\alpha(\mathbf{r})\hat{\mathbf{e}}_M^\alpha$, only the directions $\hat{\mathbf{e}}_M^\alpha$ (and consequently $m^\alpha(\mathbf{r})$) are relaxed. In order to relax the magnetic configuration it is necessary to calculate the total (integrated) perpendicular output magnetization:

$$\langle \mathbf{m}_{\perp,out}^\alpha \rangle = \int_{MT_\alpha} \mathbf{m}_{\perp,out}^\alpha(\mathbf{r})\, d^3r. \tag{12}$$

This quantity is easier to calculate than the perpendicular magnetization density $\mathbf{m}_{\perp,out}^\alpha(\mathbf{r})$, since only the spherical part, $\mathbf{m}_{\perp,out}^\alpha(r)$, of the perpendicular magnetization density is needed to calculate the integrated quantity. The integrated parallel magnetic moment is calculated just as in a collinear calculation,

$$\langle \mathbf{m}_{\parallel,out}^\alpha \rangle = M^\alpha \hat{\mathbf{e}}_M^\alpha = \int_{MT_\alpha} \mathbf{m}_{\parallel,out}^\alpha(\mathbf{r})\, d^3r = \int_{MT_\alpha} m_{\parallel,out}^\alpha(\mathbf{r})\, \hat{\mathbf{e}}_M^\alpha\, d^3r. \tag{13}$$

The output direction $\hat{\mathbf{e}}_{out}^{\alpha,(i)} = (\langle \mathbf{m}_{\perp,out}^\alpha \rangle + \langle \mathbf{m}_{\parallel,out}^\alpha \rangle)/|\langle \mathbf{m}_{\perp,out}^\alpha \rangle + \langle \mathbf{m}_{\parallel,out}^\alpha \rangle|$ at each site α differs normally from the input direction (the orientation of the spins at the beginning of the iteration step i), $\hat{\mathbf{e}}_{in}^{\alpha,(i)}$. For the next iteration $i+1$, the input direction $\hat{\mathbf{e}}_{in}^{\alpha,(i+1)}$ is changed independently of the charge density and the size of the magnetizations, $|\langle \mathbf{m}_{\perp,out}^\alpha \rangle|$ or $|\langle \mathbf{m}_{\parallel,out}^\alpha \rangle|$. In our implementation the parameters describing the orientation are the azimuthal and polar angles φ and θ, respectively. As a first and successful approach we used straight mixing to determine the input orientation for the next iteration step: For example the angle $\varphi_{in}^{\alpha,(i+1)}$ being used in the next iteration is chosen as:

$$\varphi_{in}^{\alpha,(i+1)} = (1-\beta)\, \varphi_{in}^{\alpha,(i)} \; + \; \beta\, \varphi_{out}^{\alpha,(i)}, \tag{14}$$

where β is a mixing parameter, which is chosen to obtain fast convergence. Convergence of the charge and magnetization density, and the directions can be done simultaneously, i.e. after each self-consistency iteration of the densities a new set of angles is determined. The mixing scheme as well as the mixing parameters are chosen independently for the densities and the directions. However, when a Broyden mixing scheme is used for the densities, the Broyden "memory" has to be deleted regularly (every 10 iterations) while the directions are still changing quickly.

As a test system for this implementation we have chosen fcc-Co (cf. Fig. 2), because it is well known that fcc-Co has a ferromagnetic ground state. The self-consistent determination of the relative ground-state angles between these two atoms was started using a converged charge density for the particular relative angle of $\frac{\pi}{2}$ between the orientation of the magnetic moments. Then the variation of the orientation is carried out as described above. We used $\beta = 3.0$, which means that the mixing is even more than 100% for the directions of the local moments. The change of the angle between both spins is shown in Fig. 3. From Fig. 3 it can be seen clearly, that the convergence of the orientation is very fast. In the above example the expected ferromagnetic state is reached after only 5 iterations. Due to the fast change of the directions, the charge $n(\mathbf{r})$ and magnetization density $m_{(||)}(\mathbf{r})$ are not converged anymore and further 15 iterations are needed basically to converge those quantities. After 20 iterations both, the densities and the directions are converged. This shows that by separating the orientational degrees of freedom of the magnetic moment from the charge-density and the size of the magnetization during the iteration-progress, the convergence of the orientation of spins can be considerably accelerated.

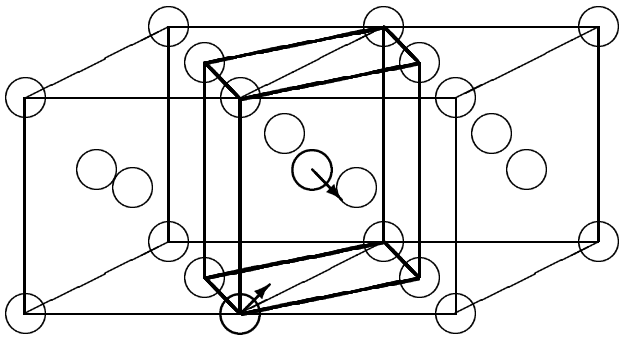

Figure 2: Fcc-lattice with the bct-unit cell (bold lines) containing two atoms. The arrows indicate the direction of the magnetic moments at each site in this unit-cell.

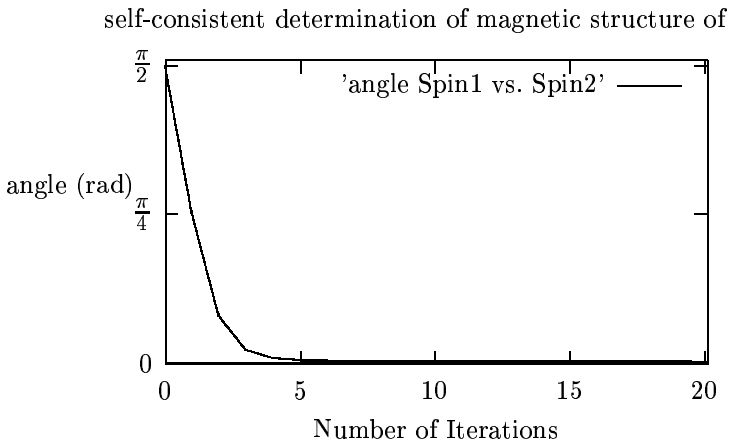

Figure 3: The calculations were performed for fcc-Co with the experimental lattice-constant of $a_0 = 6.70$ a.u. using a bct unit-cell, containing two Co-atoms. The graph shows the evolution of the relative angle between both magnetic moments (see Fig. 2.) plotted as a function of the number of iterations.

Application: Monolayers of Cr and Mn at Ag(111)

Background

In the past ultra-thin $3d$ transition-metal films, grown on oriented single-crystal noble-metal substrates, attracted much attention as they exhibit itinerant magnetism and are thus physical realizations of two-dimensional magnetic models. Most experimental and theoretical work focused on overlayers on (001) substrates. The theoretical studies [33] have predicted greatly enhanced magnetic moments in the overlayer and even more importantly two competing magnetic phases in the monolayer: the c(2×2) antiferromagnetic structure for V, Cr, and Mn monolayers and the p(1×1) ferromagnetic structure for Fe, Co, and Ni monolayers. As a result of this investigation we can conclude that the magnetic in-plane nearest-neighbor (n.n.) exchange interaction of V, Cr, and Mn is antiferromagnetic.

Antiferromagnetic interactions on a triangular lattice are the origin of frustrated spin systems. A triangular lattice is provided for example by (111) oriented fcc substrates, e.g. Ir(111) [34] or noble metals or by (0001) oriented hcp substrates, e.g. Ru(0001) [35]. The classical n.n. Heisenberg model predicts a two-dimensional non-collinear ground state for the triangular lattice, commonly called the Néel state. This configuration has three atoms in a $(\sqrt{3}\times\sqrt{3})$R30° unit cell with the magnetic moments of the three atoms aligned at $\pm 120°$ with respect to the neighboring atoms.

In fact, triangular antiferromagnets can be crystallized e.g. in the form of stacked antiferromagnets. A typical compound is $LiCrO_2$ [36] and this is a compound with *localized* spins. It seems that in many cases the magnetic interaction of localized spins are well described by the (n.n.) Heisenberg model. The systems we are investigating are *itinerant* antiferromagnets on a triangular lattice and it is by no means clear how far a short-ranged n.n. interaction or even how far the Heisenberg model can go in giving a sufficiently good description of the physics of itinerant magnets on a triangular lattice.

Therefore we investigated the ground-state spin structure of Cr and Mn monolayers beyond the Heisenberg model by performing *ab initio* calculations based on the density functional theory. We concentrate here on the discussion of unsupported (free standing) (111) monolayers (UML) of Cr and Mn with the lattice constant of Ag(111). Repeating the investigations with and without an Ag substrate does not alter the results qualitatively.

Results

The following different magnetic structures are compared: (i) The ferromagnetic p(1×1) structure. (ii) The row-wise antiferromagnetic structure as shown in Fig. 4a. The unit cell of this configuration contains 2 atoms (cf. Fig. 4c). The ferromagnetic structure and the antiferromagnetic structure is connected by a continuous rotation as indicated in Fig. 4c. (iii) The 120° configuration or the Néel state, respectively, which the n.n. Heisenberg model predicts to be energetically preferable for antiferromagnetic materials. The corresponding $(\sqrt{3}\times\sqrt{3})$R30° unit cell is shown in Fig. 4d. It is again possible to go from the ferromagnetic structure to the 120° configuration by a continuous rotation, rotating two atoms by the same angle φ but in opposite

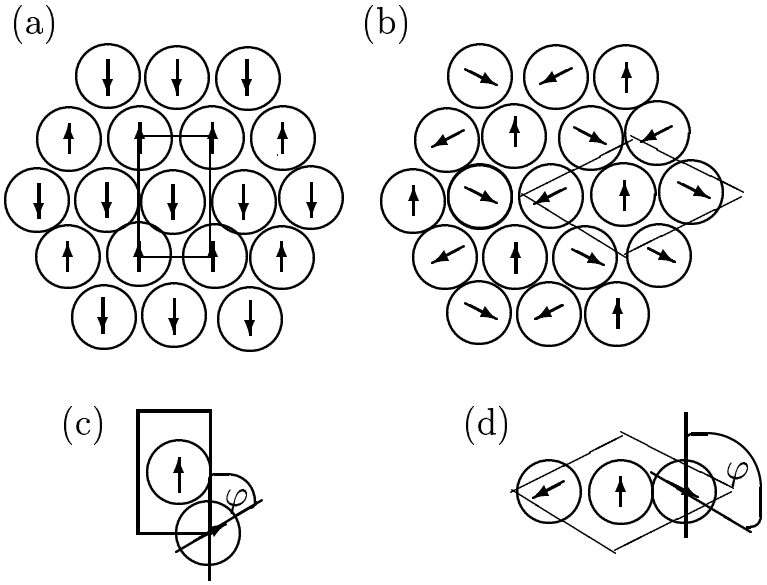

Figure 4: Magnetic structures of hexagonal monolayers: a) The row-wise antiferromagnetic structure. b) The non-collinear 120° configuration. The ferromagnetic structure can be transformed by a continuous rotation into structure a) as indicated in c) and into structure b) as indicated in d).

directions, as indicated in Fig. 4d. If this rotation is continued up to $\varphi = 180°$, the system arrives at an additional collinear antiferromagnetic structure, or more accurately an antiferrimagnetic structure, which will be denoted as the 180° configuration. A $k_{\|}$-point set that corresponds to 180 $k_{\|}$-points in the full two-dimensional Brillouin zone has been used for the unit cell containing two atoms, while the $k_{\|}$-point set for the $(\sqrt{3} \times \sqrt{3})$R30° unit cell corresponds to 121 $k_{\|}$-points in the full Brillouin zone. It has been checked very carefully that the total energy differences calculated in the two different unit cells are comparable (in particular with respect to the $k_{\|}$-point convergence), by comparing the energy difference between the non-magnetic and ferromagnetic configuration in both unit cells.

The results of the calculations are presented in Fig. 5. The plots show the total energy as a function of the rotation angle φ. The left panels show rotations that transform the ferromagnetic structure into the row-wise antiferromagnetic structure. The right panels show the rotations according to Fig. 4d. The scales of the left and right panels are equal, they differ, however, between Cr (upper panels) and Mn (lower panels).

Consider first Cr: Starting from the row-wise antiferromagnetic solution (Fig. 5 upper left panel), and rotating towards the ferromagnetic structure, the energy shows a cosine-like behavior, as the n.n. Heisenberg model predicts for an antiferromagnet. The total energy along the rotation path in the unit cell of Fig. 4d (Fig. 5 upper right panel) reveals a pronounced minimum at 120°. This minimum and shape of the energy curve matches nicely the expectation from the Heisenberg model. It is clearly visible that the 120° configuration is the lowest energy configuration among all configurations studied here. Thus, the magnetic Néel state is the ground state of the Cr UML predicted by the present investigation.

Now turning to Mn and comparing the results in the two-atom unit-cell (Fig. 5 lower left panel)

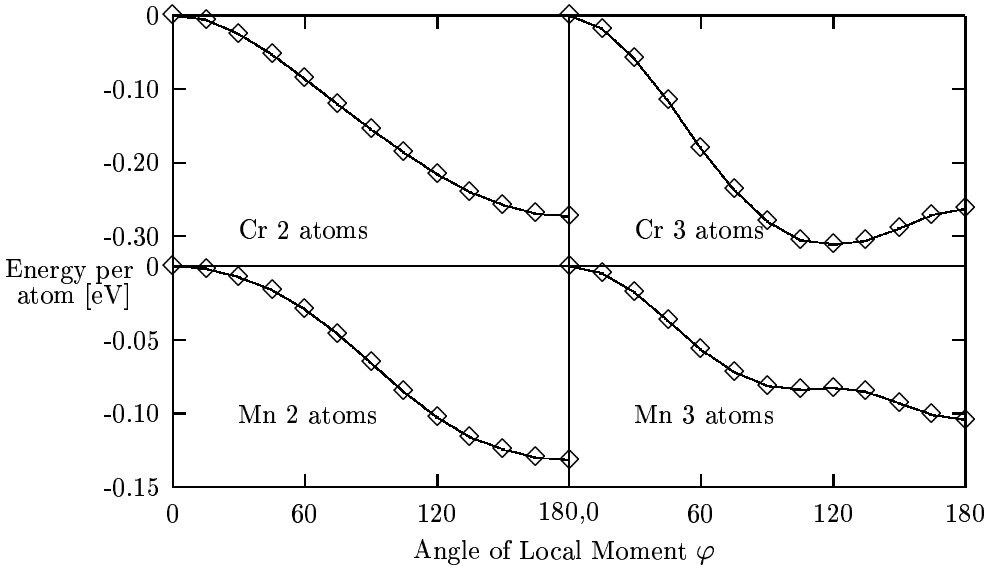

Figure 5: Calculated energy as function of the rotation angle of the local moment for the UML of Cr (upper panels) and Mn (lower panels) with the Ag(111) geometry.

with those of Cr (Fig. 5 upper left panel) we find that the behavior of Mn and Cr is very similar, i.e. the energy curve is cosine-like and Mn prefers to be antiferromagnetic. The calculations reveal, however, two surprises: (i) The lowest energy configuration among all magnetic structures investigated is the row-wise antiferromagnetic configuration. (ii) The total energy of the Mn system with 3 atoms per unit cell does not exhibit a minimum at 120°, as should be expected from the n.n. Heisenberg model, but a local maximum. Apparently, the 180° configuration is lower in energy than the Néel state (120° configuration). In summary, the lowest energy configuration, among all magnetic structures investigated, is the row-wise antiferromagnetic configuration.

From these results we can draw two conclusions:
(i) Since the row-wise antiferromagnetic configuration is lower in energy than the Néel state, the exchange interaction beyond nearest neighbors is important. Thus we cannot *a priori* exclude the possibility of even more complicated spin structures that have been ignored so far. The most probable ones are the incommensurate spin-spiral states along the high-symmetry lines in the two-dimensional Brillouin zone for the spin-spiral wave vectors. We have investigated the total energy along those high-symmetry lines and found that the row-wise antiferromagnetic state (high-symmetry point in the two-dimensional Brillouin zone) has the lowest energy among all spin-spiral wave vectors on high-symmetry lines.
(ii) Within the Heisenberg model the energy $E(\varphi)$ is either proportional to $\cos(\pm\varphi)$ or $\cos(\pm 2\varphi)$. A functional form consisting of these terms cannot fit the local maximum at 120° for Mn. Motivated by the perturbative treatment of the Hubbard-model [37] in case of strong Coulomb-interaction in which the Heisenberg Hamiltonian is derived in second order perturbation, and the lowest order correction to the Heisenberg model is due to four-spin interactions, we suggested in Ref. [38] that the maximum at 120° is due the four-spin interactions. The classical Hamiltonian

describing the four-spin interaction reads

$$H_{4\text{-}spin} = -\sum_{ijkl} K_{ijkl}[(\mathbf{S}_i\mathbf{S}_j)(\mathbf{S}_k\mathbf{S}_l) + (\mathbf{S}_j\mathbf{S}_k)(\mathbf{S}_l\mathbf{S}_i) - (\mathbf{S}_i\mathbf{S}_k)(\mathbf{S}_j\mathbf{S}_l)]. \quad (15)$$

Within the n.n. approximation ($K_{ijkl} = K_1$), the energy of the four-spin interaction in the three-atom unit-cell exhibit exactly a functional form $E(\varphi) \propto \cos 3\varphi$.

Acknowledgment

We thank Kunitomo Hirai and Leonid Sandratskii for many fruitful discussions during the course of this work. This work was supported by the Deutsche Forschungsgemeinschaft under Grant number BL444/1-1 and the TMR Networks, Contract Nos: EMRX-CT96-0089 and FMRX-CT98-0178.

References

[+] Electronic address: s.bluegel@fz-juelich.de

[1] L. M. Sandratskii and P. G. Guletskii, J. Phys. F: Met. Phys. **16**, 143 (1986).

[2] O. N. Mryasov, A. N. Lichtenstein, L. M. Sandratskii, and V. A. Gubanov, J. Phys.: Condens. Matter **3**, 7683 (1991).

[3] M. Uhl, L. M. Sandratskii, and J. Kübler, J. Magn. Magn. Mater. **103**, 314 (1992).

[4] V. P. Antropov, M. I. Katsnelson, M. van Schilfgaarde, and B. N. Harmon, Phys. Rev. Lett. **75**, 729 (1995).

[5] J. Sticht, K. H. Höck, and J. Kübler, J. Phys.: Condens. Matter **1**, 8155 (1989).

[6] J. Kübler, M. Uhl, and L. M. Sandratskii, Physica B **186-188**, 863 (1993).

[7] L. M. Sandratskii and J. Kübler, Phys. Rev. Lett. **75**, 946 (1995).

[8] R. Lorenz, J. Hafner, S. S. Jaswal, and D. J. Sellmyer, Phys. Rev. Lett. **74**, 3688 (1995).

[9] M. Liebs, K. Hummer, and M. Fähnle, Phys. Rev. B **51**, 8664 (1995).

[10] A. V. Smirnov and A. M. Bratkovsky, Europhys. Lett. **33**, 527 (1996).

[11] T. C. Schulthess, W. H. Butler, G. M. Stocks, S. Maat, and G. J. Mankey, J. Appl. Phys. **85**, 4842 (1999).

[12] A. Vega, D. Stoeffler, H. Dreysse, and C. Demangeat, Europhys. Lett. **31**, 561 (1995).

[13] V. Drchal, J. Kudrnovsky, I. Turek, and P. Weinberger, preprint

[14] O. Ivanov and V. P. Antropov, J. Appl. Phys. **85**, 4821 (1999).

[15] G. M. Stocks *et al.*, Phil. Mag. B **78**, 665 (1998).

[16] L. M. Sandratskii and J. Kübler, Newsletter 14 (1996), http://psi-k.dl.ac.uk/psi-k/highlights.html.

[17] L. M. Sandratskii, Adv. in Phys. **47**, 91 (1998).

[18] L. M. Sandratskii and P. G. Guletskii, J. Magn. Magn. Mater. **79**, 306 (1989).

[19] J. Kübler, K. H. Höck, J. Sticht, and A. R. Williams, J. Phys. F: Met. Phys. **18**, 469 (1988).

[20] J. Kübler, K. H. Höck, J. Sticht, and A. R. Williams, J. Appl. Phys. **63**, 3482 (1988).

[21] O. N. Mryasov, A. I. Lichtenstein, L. M. Sandratskii, and V. A. Gubanov, Phys. Rev. B **45**, 12330 (1992).

[22] L. Nordström and D. J. Singh, Phys. Rev. Lett. **76**, 4420 (1996).

[23] L. Nordström and A. Mavromaras, Europhys. Letters, (in press).

[24] U. von Barth and L. Hedin, J. Phys. C **5**, 1629 (1972).

[25] For a recent review see: J. Nogues, I. K. Schuller, J. Magn. Magn. Mater. **192**, 203 (1999).

[26] G.A. Prinz, Science **282**, 1660 (1998).

[27] G. Bihlmayer, S. Blügel, R. Podloucky, T. Asada, J. Redinger, M. Weinert, to be published.

[28] Ph. Kurz, PhD Thesis, to be submitted to RWTH-Aachen.

[29] P. H. Andersson, L. Nordström, and O. Eriksson, Phys. Rev. B **60**, 6765 (1999).

[30] E. Wimmer, H. Krakauer, M. Weinert, and A. J. Freeman, Phys. Rev. B **24**, 864 (1981). M. Weinert, E. Wimmer and A. J. Freeman, Phys. Rev. B **26**, 4571 (1982).

[31] P.H. Dederichs, S. Blügel, R. Zeller, and H. Akai, Phys. Rev. Lett. **53**, 2512 (1984).

[32] C. Herring, *Magnetism IV*, Chapt. V and XIII, eds. G. Rado, H. Suhl, Academic Press New York, London (1966).

[33] M. Weinert and S. Blügel, in: *Magnetic Multilayers* (eds., L. H. Bennett and R. E. Watson), World Scientific, Singapore (1993).

[34] W. L. O'Brien and B. P. Tonner, J. Vac. Sci. Technol. A **13**, 1544 (1995).

[35] A. S. Arrot, B. Heinrich, S. T. Purcell, J. F. Cochran and K. B. Urquhart, J. Appl. Phys. **61**, 3721 (1987).

[36] For recent reviews on triangular antiferromagnets see: H. Kawamura, J. Phys.: Condens. Matter **10**, 4707 (1998); M.F. Collins and O.A. Petrenko, Can. J. Phys. **75**, 605 (1997).

[37] M. Takahashi, J. Phys. C **10**, 1289 (1977).

[38] Ph. Kurz, G. Bihlmayer, K. Hirai, S. Blügel, submitted to Phys. Rev. Lett.